Int J Adv Manuf Technol (2016) 86:3443–3451
DOI 10.1007/s00170-016-8374-1

ORIGINAL ARTICLE

Quality monitoring based on dynamic resistance and principal component analysis in small scale resistance spot welding process

Xiaodong Wan[1] · Yuanxun Wang[1,2] · Dawei Zhao[1]

Received: 14 September 2015 / Accepted: 13 January 2016 / Published online: 15 February 2016

Abstract The present study aims at solving weld quality monitoring problem in small scale resistance spot welding of titanium alloy. Typical dynamic resistance curves were divided into several stages based on the weld nugget formation process. A smaller electrode force or lower welding current was found to promote the initial resistance peak. The bulk material heating stage could not be detected under very high welding current condition. Electrode force effect on dynamic resistance and failure load was much smaller than that of welding current. Principal component analysis was made on discrete dynamic resistance values. The first principal component was selected as independent variable in regression analysis for quality estimation. A back propagation neural network model was then proposed to simultaneously predict the nugget size and failure load. The electrode force, welding current, welding time, and first five principal components were designed as network inputs. Effectiveness of the developed model was validated through data training, testing, and validation. The realtime and online quality monitoring purpose could be realized.

Keywords Small scale resistance spot welding · Titanium alloy · Quality monitoring · Dynamic resistance · Principal component analysis · Artificial neural network

✉ Yuanxun Wang
wangyuanxun@hust.edu.cn

[1] Department of Mechanics, Huazhong University of Science and Technology, Wuhan 430074, China

[2] Hubei Key Laboratory for Engineering Structural Analysis and Safety Assessment, Luoyu Road 1037, Wuhan 430074, China

1 Introduction

Resistance spot welding has been widely applied in sheet joining process due to the effectiveness, easy operation, and automation. Spot welds are simply formed by the welding current introduced heat generation. Traditional "large scale" resistance spot welding (LSRSW) has been the predominant jointing procedure in automotive industry. Recently, small scale resistance spot welding (SSRSW) is drawing more attentions due to the increasing demands in miniaturized devices and components [1]. Very thin sheet metals with thickness smaller than 0.5 mm are jointed together in SSRSW.

Extensive studies have been focused on weld quality monitoring in LSRSW. Destructive testing on randomly sampled workpieces could be used to determine whether the spot weld is satisfactory. However, this off-line method is not recommended because of the cost in time, productivity, and material. The online and non-destructive techniques are thus proposed for a better solution of quality monitoring. Parameters like the dynamic resistance [2–4], electrode force [5, 6], electrode displacement [7–10], electrode temperature [11], sonic emission [12], and multi-sensor fusion [13–15] could be utilized as measured quality signals. The neural network [13, 14, 16, 17], regression analysis [18], image processing [7–9, 19], and fuzzy logic [15] could be applied in signal processing.

The power source in LSRSW is typically alternating current mode. Dynamic resistance is generally calculated using the peak current at each half cycle and voltage at that moment. Dickinson et al. [2] designed an electrical parameter monitoring system. Dynamic resistance variation was related to the nugget development. Cho et al. [3] obtained the dynamic resistance using process variables monitored in primary circuit. It was supposed effective to estimate the

weld strength. Zhou et al. [4] proposed different dynamic resistance calculation methods. Dynamic resistance curve was applied in the nugget diameter estimator to determine the first melting point.

Despite comprehensive investigations on weld quality monitoring in LSRSW, less attentions have been paid to SSRSW. Chen et al. [20] presented an empirical model to simulate the electrode displacement from monitored clamping force in SSRSW. Expulsion occurrence could be clearly identified from the displacement. Tseng et al. [21] measured the electrode displacement in SSRSW by a laser displacement sensor. The correlation between welding parameter adjustment and maximum electrode displacement variation was investigated. Nugget formation and development could be reflected from the displacement signal. Chen et al. [22] performed a finite element model on SSRSW process. The simulated maximum electrode displacement and minimum dynamic resistance were found useful in realizing real-time quality monitoring. Tan et al. [23] analyzed the dynamic resistance variation in SSRSW of bare Ni sheets. Significant differences were found between LSRSW and SSRSW. Wan et al. [24] monitored the electrode voltage signal in SSRSW. Pattern recognition of the voltage curve was applied in weld quality estimation.

High frequency inverter welding mode of direct current is generally adopted in SSRSW. Dynamic resistance could be calculated through dividing electrode voltage by welding current. In addition, titanium and its alloy possess characteristics of low density, good mechanical properties, and excellent corrosion resistance. The weldability of pure titanium under LSRSW has been proven by Kahraman and Kaya [25, 26], despite the easy activation with nitrogen and oxygen at high temperature.

There is a lack of quality monitoring research utilizing dynamic resistance in SSRSW by now. In the present study, characteristics of dynamic resistance variation in SSRSW of titanium alloy were related to the weld nugget formation process. Effects of welding parameters on dynamic resistance and mechanical properties of spot welds were analyzed. Principal component analysis (PCA) was conducted on measured dynamic resistance curve. The principal components were used as independent variables in regression analysis and neural network model to realize an effective quality estimation.

2 Methodologies

2.1 Principal component analysis (PCA)

The PCA was first proposed by Pearson [27] and Hotelling [28]. It is an effective tool in dimension reduction, and the original information could be kept as much as possible. All principal components are orthogonal to each other. The procedure could be described as follows:

Step 1: Calculation of correlation coefficient array $\boldsymbol{R}$.

$$r_{st} = \frac{\mathrm{cov}(x_s(j), x_t(j))}{\sigma_{x_s(j)} \times \sigma_{x_t(j)}} \tag{1}$$

where $\mathrm{cov}(x_s(j), x_t(j))$ is the covariance of sequences $x_s(j)$ and $x_t(j)$. $\sigma_{x_i(j)}$ is the standard deviation of sequence $x_i(j)$. The original array is represented by $\boldsymbol{X}$:

$$\boldsymbol{X} = \begin{pmatrix} x_1(1) & x_2(1) & \dots & \dots & x_m(1) \\ x_1(2) & x_2(2) & \dots & \dots & x_m(2) \\ \vdots & \vdots & \vdots & \vdots & \vdots \\ x_1(n) & x_2(n) & \dots & \dots & x_m(n) \end{pmatrix}$$

where m is the number of characteristics, n is the number of experiments.

Step 2: Calculation of the eigenvalues and eigenvectors.

$$(\boldsymbol{R} - \lambda \boldsymbol{E})\, V = \boldsymbol{0} \tag{2}$$

where λ is the eigenvalue of $\boldsymbol{R}$, V is the corresponding eigenvector.

Step 3: Calculation of principal component scores.

$$pc_k(j) = \sum_{i=1}^{m} x_i(j) \times v_k(i) \tag{3}$$

where $pc_k(j)$ is the jth component of kth principal component, $v_k(i)$ is the ith component of kth eigenvector.

2.2 Back propagation neural network (BPNN)

Neural network is designed to imitate the brain's processing capability. Neuron is the fundamental constituent part. Neural network analysis is cost effective, easy to understand, and has been employed in the manufacturing process. BPNN is one of the commonly used neural networks, by which a complicated nonlinear relationship between inputs and outputs could be mapped. It belongs to the supervised learning model. Training procedure is necessary to construct the relationship. It has a multi-layer feed-forward structure with one input layer, one or more hidden layers, and one output layer.

Neurons are linked together by weights and biases which could convey data from previous layer to the next. The weight that connects neuron j in layer k to neuron i in layer $k+1$ is termed as w_{ij}. The bias of neuron i in layer $k+1$

Table 1 The chemical composition of TC2 titanium alloy, wt%

Alloying elements			Impurities (not higher than)					
Al	Mn	Ti	Fe	C	N	H	O	Others
3.5 ∼ 5.0	0.8 ∼ 2.0	Bal.	0.30	0.10	0.05	0.012	0.15	0.40

is characterized by θ_i. Input value of each neuron in layer $k+1$ is:

$$net_i = \sum_{j=1}^{p} \omega_{ij} x_j + \theta_i \tag{4}$$

where x_j is the output data of neuron j in layer k, p is the number of neurons in layer k. Output value of each neuron in layer $k+1$ could be determined as:

$$out_i = f(net_i) \tag{5}$$

where f is the linear, log-sigmoid, or hyperbolic tangent sigmoid transfer function. Weights and biases are iteratively adjusted in training procedure to minimize the total mean square error. The training procedure of BPNN could be summarized as follows:

Step 1: Initialization of weights and biases.
Step 2: Select inputs from training set and calculate outputs with the neural network.
Step 3: Adjust weights and biases to reduce the total mean square error.
Step 4: Return to *Step 2*.
Step 5: Stop training when the stopping criterion is satisfied.

3 Experimental procedure

TC2 titanium alloy with a thickness of 0.4 mm was prepared for SSRSW. Chemical composition of the material is listed in Table 1. TC2 sheets were cut into dimensions of 100 × 30 mm, as shown in Fig. 1. Mechanical and chemical cleaning were both adopted before welding. A hard brush was employed in mechanical cleaning to roughly clear contaminants at the sheet surface. Then samples were etched with a mixed solution of nitric acid, hydrofluoric acid, and water for several minutes. After cleaned by running water at room temperature, specimens were placed in a ventilated environment.

The SSRSW machine utilized was produced by Miyachi Unitek Corporation, as depicted in Fig. 2. The welding machine was designed to work under high frequency inverter power supply mode. Spot weld could be made under constant current, constant voltage, and constant power welding conditions. Constant welding current mode was utilized here due to the better adaptability. A typical welding current curve is illustrated in Fig. 3. Tip diameter of the electrode was 3.0 mm. No cooling water was provided during the welding process. Electrode force (F) was varied between 100 and 200 N, welding current (I) was varied between 1.2 and 2.4 kA, and welding time (T) was varied between 6 and 12 ms. Welding parameter combination was randomly selected and distributed as uniform as possible. A total of 60 samples were performed at last.

An illustration of the data acquisition system is given in Fig. 4. Voltage drop between electrodes during the welding process was measured directly by clipped probes. A Rogowski coil was used to obtain the welding current signal. Signal-carrying leads were all twisted to minimize the induced electromagnetic noise. Both signals were then transmitted to a computer data processing system at a fixed sampling frequency. Acquired signals were filtered and noise reduced. The electrode voltage and welding current

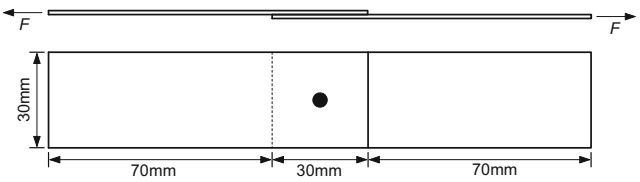

Fig. 1 Specimen dimensions for SSRSW

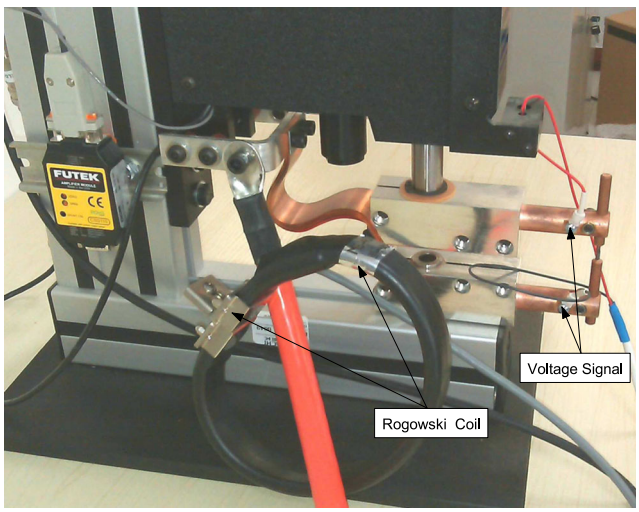

Fig. 2 The SSRSW machine

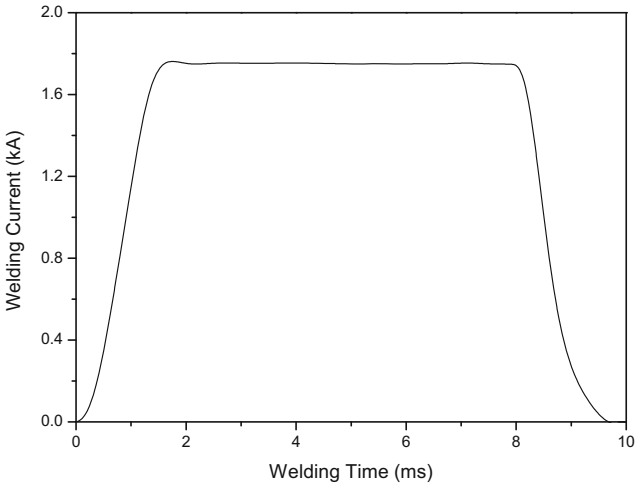

Fig. 3 Typical welding current curve

curves could be acquired online after corresponding data processing. The dynamic resistance could then be calculated through dividing electrode voltage by welding current.

As the nugget size variation in SSRSW was limited, weld quality characteristics were selected as nugget size and failure load. Quasi-static tensile-shear tests on spot welded specimens were conducted with an Instron universal testing machine. Cross-head speed was kept constant at 1.0 mm/min. Failure load was referred to the peak value of load-displacement curve. Nugget size was obtained by a vernier caliper on fractured welding surface.

4 Results and discussion

4.1 Typical dynamic resistance curve analysis

Two typical dynamic resistance curves obtained in experiments are shown in Fig. 5. Mode A curve is acquired under normal welding condition of F = 200 N, I = 1.6 kA, and T = 8 ms. It could be divided into four stages based on characteristics of resistance variation. They are the (I) asperity heating, (II) surface breakdown and softening, (III) bulk material heating, and (IV) nugget formation stages. An initial γ resistance peak around 1.75 mΩ could be observed. The γ peak is defined to distinguish from the α valley and β peak obtained in dynamic resistance analysis of LSRSW [2]. It could be explained by initial heating of asperities, while the bulk material is still cool. The overall temperature at stage I is supposed very low [23]. Lack of this stage in LSRSW may be due to selection of alternating current.

The dynamic resistance drops obviously at stage II, which is probably related to the electrical and mechanical film breakdown caused by electrode voltage and electrode force, respectively. Sheet to sheet contact is established after the surface breakdown. The further decrease in dynamic resistance is introduced by softening behavior of asperities and enlargement of contact area. Heat generation is concentrated at contact interfaces, and the temperature of corresponding positions is increased significantly. Resistivity of the bulk material increases with temperature at the same time. The dynamic resistance variation is a result of the above-mentioned competitive mechanisms. The resistance decreasing mechanism plays a dominant role at this stage. Dynamic resistance continues to drop at a much lower rate. A balance is eventually reached at the end of stage II, which accounts for the α valley.

The overall resistance begins to rise at stage III due to the sustained bulk material heating. Contact resistance is gradually disappeared at this stage. Local melting of the sheet to sheet contact surface should have occurred at the deflection point ($d^2R/d^2t = 0$) of stage III. After the deflection point, cross-sectional area for welding current passage is gradually increased due to the successive melting at contact interfaces. Mechanical collapse caused by material softening and electrode pressure would shorten the current flow path. They both lead to the dynamic resistance reduction. Temperature field of melted region is gradually stabilized,

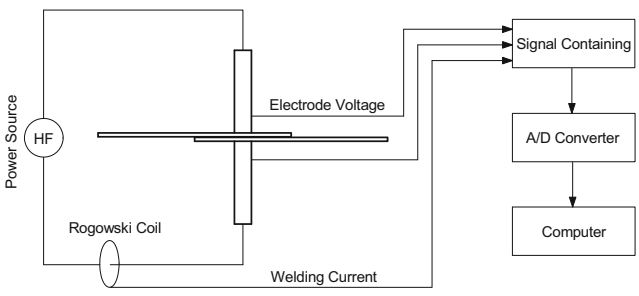

Fig. 4 Illustration of the data acquisition system

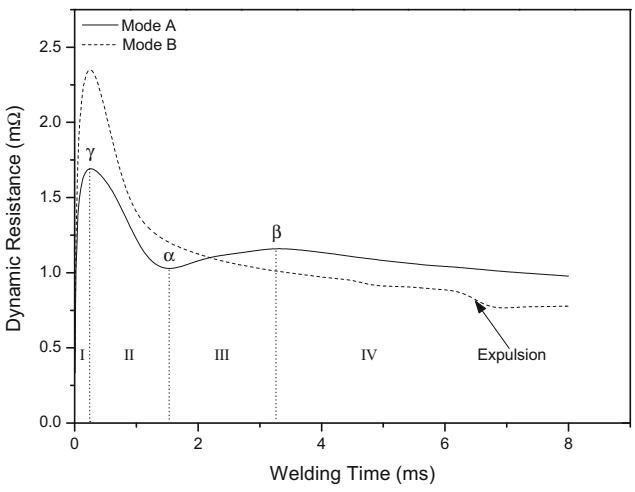

Fig. 5 Two different dynamic resistance curve modes

and the dynamic resistance increase due to bulk material heating is restricted. A β peak is thus formed at the end of stage III. The β peak roughly reveals when the weld nugget grows to an acceptable size. At stage IV, material melting and mechanical collapse dominate the resistance variation tendency. A consistent resistance decrease until the welding end could be observed.

Dynamic resistance curve of mode B is obtained under F = 75 N, I = 2.4 kA, and T = 8 ms welding condition, which is obviously different from that of mode A. The electrode force is much smaller and welding current is much higher. An initial resistance peak of about 2.25 mΩ at stage I could be found. The larger γ peak value could be attributed to the smaller electrode force. A more intensive current density is existed under this welding condition, which introduces more initial heat generation and a larger γ peak. The nugget formation and development in mode B are much earlier and faster than that in mode A. Dynamic resistance decreasing capability is thus enhanced in mode B. The typical stage III could not be detected then. Besides, expulsion occurrence could be deduced from the sudden drop of dynamic resistance.

4.2 Effect of welding parameters on dynamic resistance and failure load

The effect of welding parameters on dynamic resistance is depicted in Fig. 6. All the welding time is kept constant at 8 ms. The electrode force effect on dynamic resistance curve is shown in Fig. 6a. Welding current is maintained at 2.0 kA. As could be seen, the γ peak value decreases as electrode force increases. This is due to the fact that more asperities are in contact under a larger electrode force, which leads to a smaller current density. The initial heating capability is thus decreased at stage I. Increasing tendency of asperity resistivity with temperature is reduced as a consequence. However, the difference in dynamic resistance variation at following stages is very small, including characteristics of α valley, β peak, and end resistance. In fact, the dynamic resistance variation is closely related to heat generation. The heat generation during welding process is controlled by the formula $Q = I^2RT$, in which the welding current plays a dominant role. The dynamic resistance variation is closely related to heat generation. Considering the same welding current condition, it is not surprising to observe the nearly identical trend of dynamic resistance curve. It could also be deduced that the electrode force effect on heat generation is limited.

The influence of welding current on dynamic resistance variation is given in Fig. 6b, in which the electrode force is kept constant at 150 N. It could be found that dynamic resistance variation is more sensitive to welding current than electrode force. A significant decrease in the overall dynamic resistance level could be observed as welding

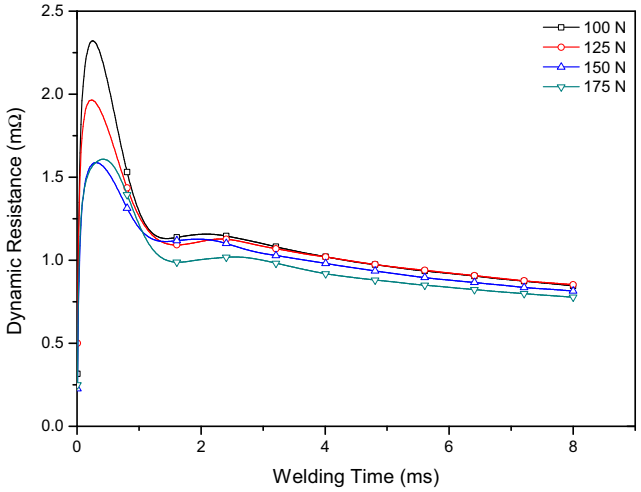

(a) Electrode force effect (I = 2.0 kA)

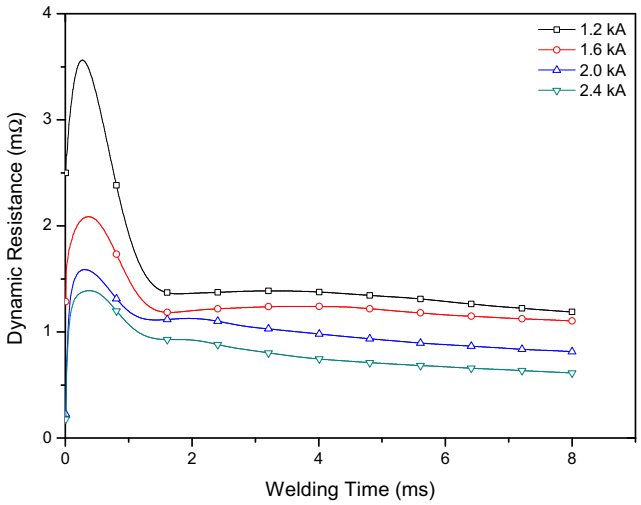

(b) Welding current effect (F = 150 N)

Fig. 6 Effect of welding parameters on dynamic resistance curve

current increases, which could be explained by the larger nugget size and more mechanical collapse. As welding current increases, bulk resistance increasing rate is gradually smaller than resistance decreasing rate introduced by nugget growth. The β peak position is thus moved forward and difference between α valley and β peak is reduced. Besides, the end resistance is smaller under higher welding current condition.

Welding parameter influence on failure load of spot welded specimens is shown in Fig. 7. Welding time is varied from 6 to 12 ms. The constant welding current and electrode force setup are the same as that in Fig. 6. Failure load is increased with welding time due to the increasing fusion zone formed by heat generation. As could be seen from Fig. 7a, the electrode force effect on failure load is not obvious, which is similar to the conclusion in dynamic resistance analysis. Influence of welding current on failure load is

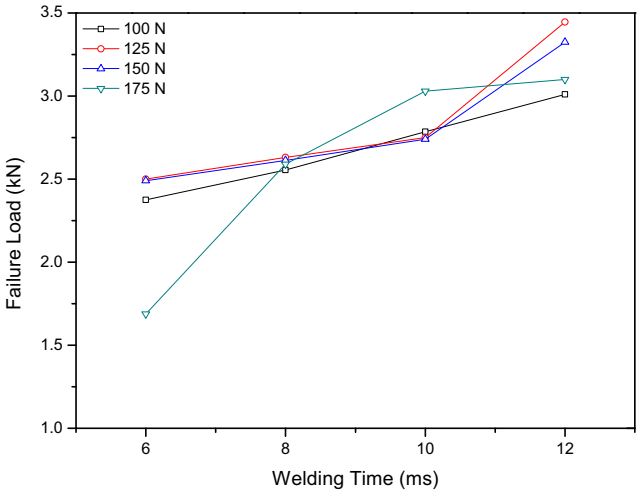

(a) Electrode force effect (I = 2.0 kA)

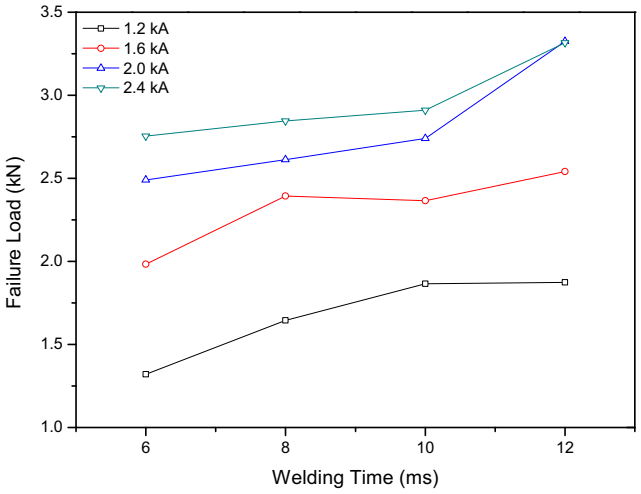

(b) Welding current effect (F = 150 N)

Fig. 7 Welding parameters influence on failure load of spot welded specimens

remarkable. A higher welding current generally indicates a larger failure load, although the increasing rate is gradually slowed, as depicted in Fig. 7b. The difference of dynamic resistance under various welding current conditions is also significant in Fig. 6b. An interrelationship could be found existed between dynamic resistance curve and failure load. The dynamic resistance could be applied as an indicator for weld quality monitoring in SSRSW.

4.3 Principal component analysis and linear regression analysis

Dynamic resistance values at specified time interval of 0.2 ms are utilized as original quality indicators. Different welding time of 6, 8, 10, and 12 ms is adopted in the study. In order to ensure the same data dimension for PCA, additional dynamic resistance values equal to the end resistance are used as a supplement for 6, 8, and 10 ms welding time conditions. A total of 61 data points are thus extracted from each dynamic resistance curve. A randomly selected 50 samples are first used to establish the regression model. The remaining 10 samples are adopted for validation purpose in regression analysis. Since the data set are approximately at the same order of magnitude, there is no need to conduct data normalization before PCA. PCA is thus implemented directly on the selected 50 samples according to previously developed procedure. Principal component scores of each sample could be obtained. The remaining 10 samples are added to the 50 samples one at a time. The principal component scores obtained are used for model validation.

PCA is conducted using the MATLAB software. Results of PCA on training data set show that accountability proportion of the first principal component (PC_1) is 78.3 %, and cumulative accountability proportion of the first five principal components reaches 99.6 %, as listed in Table 2. Effect of the PC_1 on nugget size and failure load is given in Fig. 8. The linear fit is represented by a solid line. A good linear correlation could be found between weld quality characteristics and the PC_1. Regression equations could thus be established based on the PC_1 for a rough estimation of weld quality characteristics. Equations 6 and 7 could be used to predict nugget size and failure load, respectively. For samples varied only in welding time, the difference in PC_1 may be limited when dynamic resistance variation at stage IV is very small. The welding time term is thus included into regression equations as well.

$$\text{Nugget Size} = 1.4800 - 0.1472PC_1 + 0.0351T \quad (6)$$

$$\text{Failure Load} = 1.8253 - 0.2840PC_1 + 0.0576T \quad (7)$$

Model effectiveness is validated by the remaining 10 samples, as shown in Fig. 9. Comparison results between predicted and measured responses are basically satisfactory. Simplicity is main advantage of the developed regression

Table 2 Principal component analysis

Principal component	PC_1	PC_2	PC_3	PC_4	PC_5
Eigenvalue (-)	2.0043	0.4560	0.0520	0.0292	0.0078
Proportion (%)	78.3	17.8	2.0	1.1	0.4
Cumulative (%)	78.3	96.1	98.1	99.2	99.6

model. However, only the PC_1 and welding time are considered in regression analysis. In practice, a complex relationship is existed between welding parameters and quality characteristics. A neural network model is thus performed in the following section, which has been proven effective in dealing with complicated nonlinear relationship between independent variables and multiple responses.

4.4 Back propagation neural network (BPNN) analysis

An illustration of the BPNN used in this study is shown in Fig. 10. Neural network inputs are selected considering potential quality influencing factors, including the electrode force, welding current, welding time, and first five principal components. Nugget size and failure load are utilized as network outputs. Determination of the network architecture is an important task in neural network analysis. One single hidden layer is generally adequate to approximate most continuous mapping. Selection of neuron number in the hidden layer should be taken carefully. Although prediction precision could be improved with a large number of neurons in hidden layer, the over fitting chance is increased as well. There is no such criterion to determine the neuron number in hidden layer by now. The trial and error method is generally adopted in establishing a suitable network structure.

MATLAB neural network toolbox is applied in the simulation. The 50 samples used in regression model establishment are considered first. A data set of 40 samples are randomly selected from the 50 ones for neural network model training, and the remaining 10 samples are adopted for testing purpose. The last 10 samples utilized in regression model validation are designed for neural network model validation. After many trial and error attempts including training, testing, and validation, the three layer 8–20–2 structure shows the best performance. Hyperbolic tangent sigmoid and linear transfer functions are used in the hidden

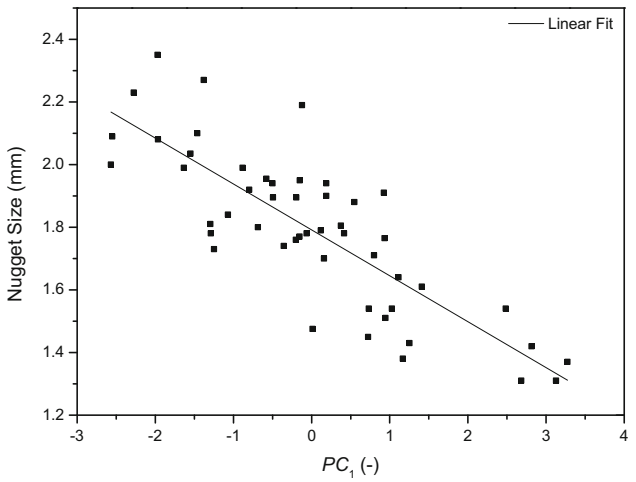

(a) Nugget size

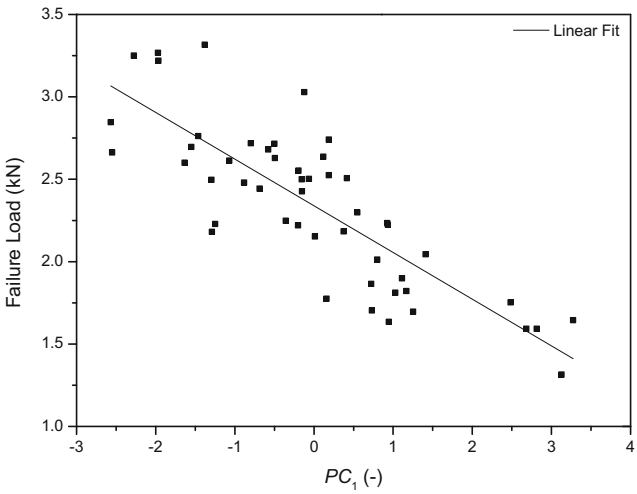

(b) Failure load

Fig. 8 Effect of the PC_1 on weld quality characteristics

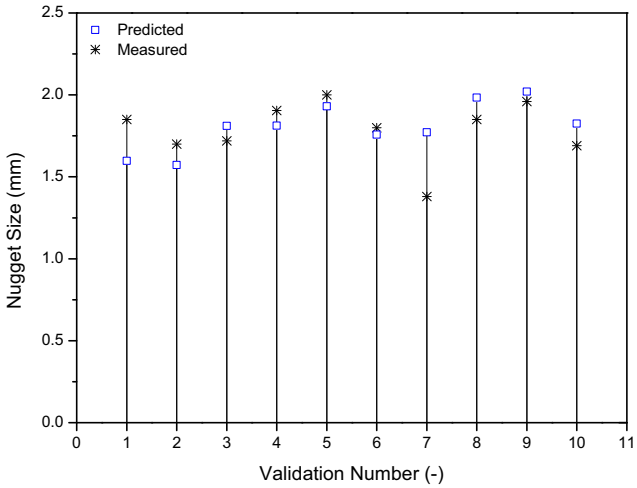

(a) Nugget size

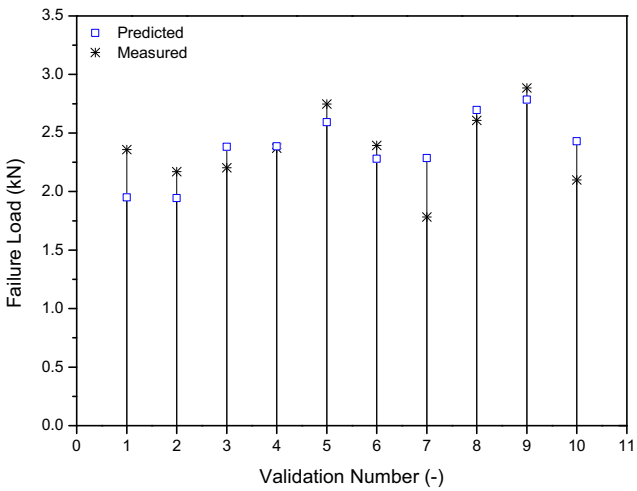

(b) Failure load

Fig. 9 Validation of the regression analysis model

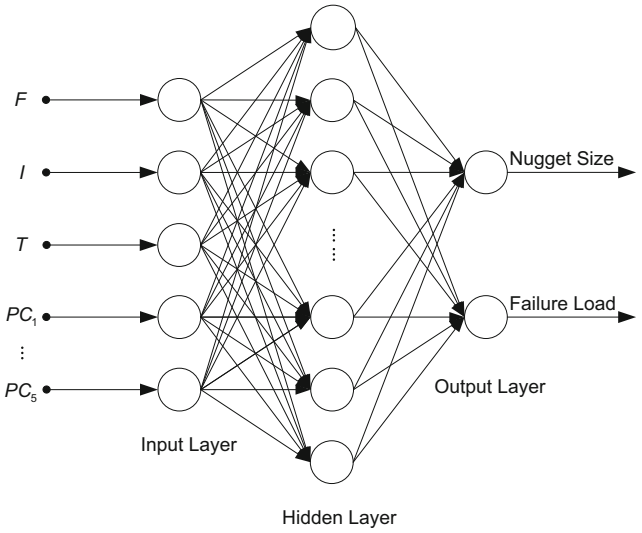

Fig. 10 Architecture of the BPNN model

and output layers, respectively. Weight and bias values are updated by the Levenberg-Marquaardt algorithm.

A scatter plot of measured weld quality characteristics versus predicted ones by the developed BPNN is depicted in Fig. 11. Results of training, testing, and validation are illustrated with different marks. Reliability of training procedure is verified from the perfect training performance. Prediction errors of nugget size and failure load in both testing and validation approaches are at an acceptable level, through which the model effectiveness is validated.

Additionally, weld quality could be classified into three levels according to the failure load magnitude. Here, the 2.0 and 3.0 kN are selected as threshold values for different levels. Corresponding threshold nugget sizes are roughly at 1.6 and 2.2 mm. The spot weld at level III is unsatisfactory due to the low failure load magnitude. Expulsion occurrence is easy to be detected for level I spot weld, although the mechanical performance is very good. The level II spot weld is supposed satisfactory at both failure load and surface quality. Estimation accuracy of the proposed model based on quality level classification is satisfactory despite several error predictions, as shown in Fig. 11.

The developed neural network model is proved effective in simultaneous estimation of nugget size and failure load. More experimental data are needed to improve the model accuracy, which means the increase of testing costs in production environment. In fact, a rough estimation of weld quality level is generally enough for engineers. Real-time quality monitoring purpose could probably be achieved, considering the very short time consumption in BPNN. Online measurement of the dynamic resistance signal and principal components could also be realized conveniently. The developed BPNN is supposed suitable for real-time and online weld quality monitoring in SSRSW of titanium alloy.

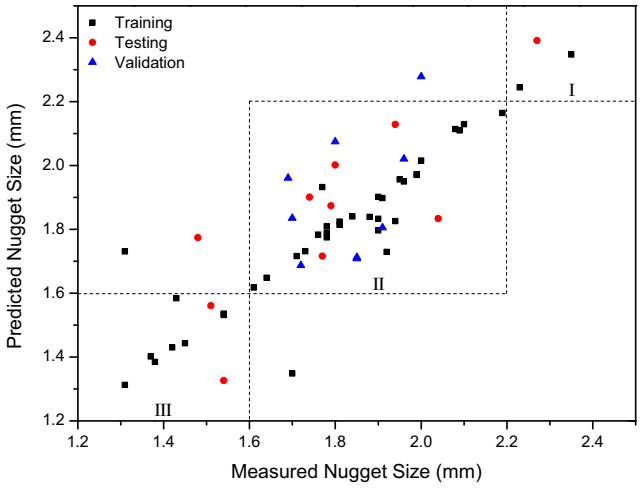

(a) Nugget size

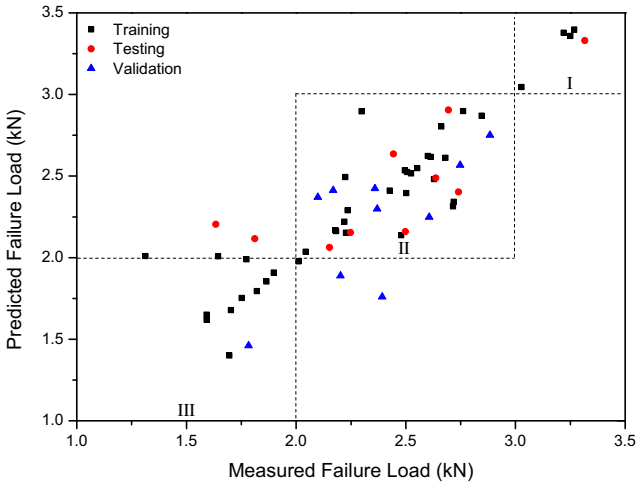

(b) Failure load

Fig. 11 Predicted versus measured weld quality characteristics by the BPNN

5 Conclusions

The weld quality monitoring approach based on dynamic resistance signal in SSRSW was conducted in this study. Dynamic resistance curve was first divided into four stages relating to the nugget formation process. Effect of welding parameters on dynamic resistance and failure load was analyzed. PCA was then made on discrete dynamic resistance values for a preliminary weld quality prediction. A BPNN analysis was also performed to estimate nugget size and failure load simultaneously. Model effectiveness was proved after data training, testing, and validation. A real-time and online weld quality monitoring system in SSRSW could be developed. Following conclusions are obtained:

– The initial γ resistance peak could be promoted under a smaller electrode force or lower welding current condition.

- Variations of dynamic resistance and failure load are more sensitive to welding current than electrode force.
- The quality level classification technique adopted in BPNN is practical for quality monitoring.

Acknowledgements This research work was funded by the National Natural Science Foundation of China (No. 11072083) and the Doctoral Dissertation Innovation Fund of Huazhong University of Science & Technology (No. 0118240059). The authors would like to thank Zongguo Lin and Suning Sheng from Miyachi Unitek Corporation for providing the welding machine. Experimental support from the Analysis and Testing Centre of Huazhong University of Science & Technology is also acknowledged.

Compliance with Ethical Standards

Disclosure of potential conflicts of interest:

Funding This research work was funded by the National Natural Science Foundation of China (No. 11072083). This research work was also funded by the Doctoral Dissertation Innovation Fund of Huazhong University of Science &Technology (No. 0118240059).

Conflict of interests The authors declare that they have no competing interests.

References

1. Wan X, Wang Y, Zhao D (2015) Multi-response optimization in small scale resistance spot welding of titanium alloy by principal component analysis and genetic algorithm. Int J Adv Manuf Technol. doi:10.1007/s00170-015-7545-9
2. Dickinson D, Franklin J, Stanya A (1980) Characterization of spot welding behavior by dynamic electrical parameter monitoring. Weld J 59(6):170–176
3. Cho Y, Rhee S (2002) Primary circuit dynamic resistance monitoring and its application to quality estimation during resistance spot welding. Weld J 81(6):104–111
4. Zhou K, Cai L (2013) Online nugget diameter control system for resistance spot welding. Int J Adv Manuf Technol 68(9-12):2571–2588. doi:10.1007/s00170-013-4886-0
5. El-Banna M, Filev D, Tseng F (2011) Force-based weld quality monitoring algorithm. Int J Intell Syst Technol Appl 10(1):1–14
6. Podržaj P, Simončič S (2013) Welding force as a variable in resistance spot welding control. In: 2nd International Conference on Measurement, Information and Control (ICMIC), Harbin, China, 16-18 Aug, pp 818–821
7. Podržaj P, Simončič S (2012) Image-based electrode tip displacement in resistance spot welding. Meas Sci Technol 23:1–7. doi:10.1088/0957-0233/23/6/065401
8. Podržaj P, Simončič S (2014) Resistance spot weld strength estimation based on electrode tip displacement/velocity curve obtained by image processing. Sci Technol Weld Join 19(6):468–475. doi:10.1179/1362171814Y.0000000212
9. Podržaj P, Simončič S (2014) A machine vision-based electrode displacement measurement. Weld World 58(1):93–99. doi:10.1007/s40194-013-0086-7
10. Zhang H, Hou Y, Zhang J, Qi X, Wang F (2015) A new method for nondestructive quality evaluation of the resistance spot welding based on the radar chart method and the decision tree classifier. Int J Adv Manuf Technol 78(5-8):841–851. doi:10.1007/s00170-014-6654-1
11. Podržaj P, Simončič S (2013) Resistance spot welding control based on the temperature measurement. Sci Technol Weld Join 18(7):551–557. doi:10.1179/1362171813Y.0000000131
12. Podržaj P, Polajnar I, Diaci J, Kariž Z (2005) Estimating the strength of resistance spot welds based on sonic emission. Sci Technol Weld Join 5(4):699–405. doi:10.1179/174329305X44107
13. Podržaj P, Polajnar I, Diaci J, Kariž Z (2004) Expulsion detection system for resistance spot welding based on a neural network. Meas Sci Technol 15:592–598. doi:10.1088/0957-0233/15/3/011
14. Cullen J, Athi N, Al-Jader M, Johnson P, Al-Shamma'a A, Shaw A, El-rasheed A (2008) Multisensor fusion for on line monitoring of the quality of spot welding in automotive industry. Mesaurement 41(4):412–423. doi:10.1016/j.measurement.2007.01.006
15. Podržaj P, Simončič S (2011) Resistance spot welding control based on fuzzy logic. Int J Adv Manuf Technol 52:959–967. doi:10.1007/s00170-010-2794-0
16. Lee H, Wang M, Maev R, Maeva E (2003) A study on using scanning acoustic microscopy and neural network techniques to evaluate the quality of resistance spot welding. Int J Adv Manuf Technol 22(9-10):727–732. doi:10.1007/s00170-003-1599-9
17. El-Banna M, Filev D, Chinnam R (2008) Online qualitative nugget classification by using a linear vector quantization neural network for resistance spot welding. Int J Adv Manuf Technol 36(3-4):237–248. doi:10.1007/s00170-006-0835-5
18. Lai X, Luo A, Zhang Y, Chen G (2009) Optimal design of electrode cooling system for resistance spot welding with the response surface method. Int J Adv Manuf Technol 41(3-4):226–233. doi:10.1007/s00170-008-1478-5
19. Ruisz J, Biber J, Loipetsberger M (2007) Quality evaluation in resistance spot welding by analysing the weld fingerprint on metal bands by computer vision. Int J Adv Manuf Technol 33(9-10):952–960. doi:10.1007/s00170-006-0522-6
20. Chen J, Farson D, Ely K, Frech T (2006) Modeling small-scale resistance spot welding machine dynamics for process control. Int J Adv Manuf Technol 27(7-8):672–676. doi:10.1007/s00170-004-2238-9
21. Tseng K, Chuang K (2012) Monitoring nugget size of micro resistance spot welding (micro RSW) using electrode displacement-time curve. Adv Mater Res 463-464:107–111. doi:10.4028/www.scientific.net/AMR.463-464.107
22. Chen Y, Tseng K, Cheng Y (2012) Electrode displacement and dynamic resistance during small-scale resistance spot welding. Adv Sci Lett 11(1):72–79. doi:10.1166/asl.2012.2180
23. Tan W, Zhou Y, Kerr H, Lawson S (2004) A study of dynamic resistance during small scale resistance spot welding of thin Ni sheets. J Phys D-Appl Phys 37(14):1998–2008. doi:10.1088/0022-3727/37/14/017
24. Wan X, Wang Y, Zhao D (2015) Quality evaluation in small scale resistance spot welding by electrode voltage recognition. Sci Technol Weld Join. doi:10.1080/13621718.2015.1115161
25. Kahraman N (2007) The influence of welding parameters on the joint strength of resistance spot-welded titanium sheets. Mater Des 28(2):420–427. doi:10.1016/j.matdes.2005.09.010
26. Kaya Y, Kahraman N (2012) The effects of electrode force, welding current and welding time on the resistance spot weldability of pure titanium. Int J Adv Manuf Technol 60(1-4):127–134. doi:10.1007/s00170-011-3604-z
27. Pearson K (1901) On lines and planes of closest fit to systems of points in space. Philos Mag Series 2(11):559–572
28. Hotelling H (1933) Analysis of a complex of statistical variables into principal components. J Educ Psychol 24(6):417–441